

# Fully Sparse 3D Panoptic Occupancy Prediction

Haisong Liu<sup>1†</sup> Haiguang Wang<sup>1</sup> Yang Chen<sup>1</sup> Zetong Yang<sup>2</sup>  
Jia Zeng<sup>2</sup> Li Chen<sup>2</sup> Limin Wang<sup>1,2</sup>   
<sup>1</sup> Nanjing University <sup>2</sup> Shanghai AI Lab

## Abstract

Occupancy prediction plays a pivotal role in the realm of autonomous driving. Previous methods typically construct a dense 3D volume, neglecting the inherent sparsity of the scene, which results in a high computational cost. Furthermore, these methods are limited to semantic occupancy and fail to differentiate between distinct instances. To exploit the sparsity property and ensure instance-awareness, we introduce a novel fully sparse panoptic occupancy network, termed SparseOcc. SparseOcc initially reconstructs a sparse 3D representation from visual inputs. Subsequently, it employs sparse instance queries to predict each object instance from the sparse 3D representation. These instance queries interact with 2D features via mask-guided sparse sampling, thereby circumventing the need for costly dense features or global attention. Additionally, we have established the first-ever vision-centric panoptic occupancy benchmark. SparseOcc demonstrates its efficacy on the Occ3D-nus dataset by achieving a mean Intersection over Union (mIoU) of 26.0, while maintaining a real-time inference speed of 25.4 FPS. By incorporating temporal modeling from the preceding 8 frames, SparseOcc further improves its performance, achieving 30.9 mIoU without whistles and bells. Code will be made available.

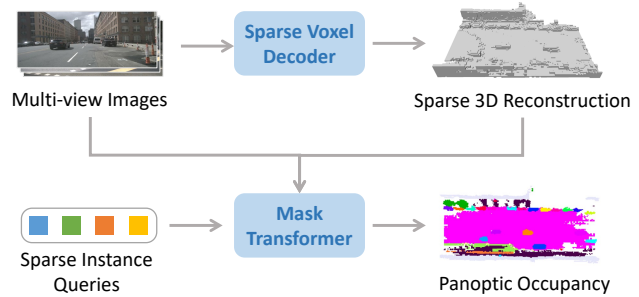


Figure 1. Overview of SparseOcc. A sparse voxel decoder reconstructs a sparse 3D representation from input images. Next, a set of sparse instance queries are used to estimate the mask and label of each instance, thus unifying semantic and instance occupancy to panoptic occupancy at the same time.

real-time requirement of autonomous driving (running 2 ~ 3 fps on a modern GPU). Although some methods [21, 23] more or less utilize the sparsity of the 3D scene, they still rely on a sparse-to-dense module to complete the scene and make dense predictions. In addition, these methods only target semantic occupancy and cannot distinguish between different instances.

In this paper, we dive into the sparsity of the scene in autonomous driving. As illustrated in Fig. 2, we believe that the sparsity should be in *two* aspects: 1) geometry sparsity. More than 90% of the voxels are empty. 2) instance sparsity. A small number of queries (e.g. 200) is enough to predict all objects around the vehicle.

Based on the above property, we propose SparseOcc, a fully sparse panoptic occupancy network. SparseOcc consists of two steps. First, we propose a *sparse voxel decoder* to reconstruct the sparse geometry of the scene. It only models the non-free regions of the scene, thereby saving computational resources significantly. Second, we design a *mask transformer* which uses sparse instance queries to predict the mask and label of each object from the sparsified space. Moreover, we further propose *mask-guided sparse sampling* to avoid the dense cross attention in mask

## 1. Introduction

Vision-centric 3D occupancy prediction [1] is designed to partition the 3D scene into structured grids. Each grid is assigned a label that indicates whether it is occupied. 3D occupancy offers more geometric detail than 3D bounding boxes and can be used as an alternative to LiDAR-based representations [18, 25, 30, 51–53].

Existing methods [14, 22, 23, 41, 50] typically require constructing a dense 3D feature, which cannot meet the

Ongoing project. Content may change.

†: Work partly done during an internship at OpenDriveLab.

: Corresponding author.

transformer. As such, our SparseOcc can exploit both the sparse properties mentioned above simultaneously, forming a fully sparse architecture since it neither relies on dense 3D feature, nor has sparse-to-dense and global attention operations. At the same time, SparseOcc can distinguish between different instances in the scene, unifying semantic occupancy and instance occupancy into panoptic occupancy.

Besides, we create the first vision-centric panoptic occupancy benchmark and use the Panoptic Quality (PQ) metric [17] to evaluate the performance. The panoptic occupancy benchmark is based on existing semantic occupancy benchmarks such as Occ3D-nus [45], OpenOcc [41], etc.

Thanks to the sparsity design, SparseOcc achieves a real-time inference speed of 25.4 FPS<sup>1</sup>, while maintaining 26.0 mIoU on Occ3D-nus. After adding the temporal modeling of the past 7 frames, SparseOcc can achieve 30.9 mIoU, achieving state-of-the-art performance on Occ3D-nus without whistles and bells.

Our contributions are three-fold:

1. We propose the first fully sparse model for (panoptic) 3D occupancy prediction.
2. Our model, named SparseOcc, uses sparse voxel decoder to exploit geometry sparsity and sparse instance queries to exploit object sparsity.
3. Based on the proposed vision-centric panoptic occupancy benchmark, we demonstrate the effectiveness of SparseOcc in terms of both speed and accuracy.

## 2. Related Work

**Camera-based 3D Object Detection.** Camera-based 3D object detection plays a crucial role in BEV perception [19, 20]. Existing methods in this domain can be generally classified into two categories: dense BEV-based methods [13, 14, 22, 35] and sparse query-based methods [26–28, 49]. BEVFormer [22] designs a transformer-based network consisting of spatial cross-attention and temporal self-attention to aggregate spatio-temporal information. BEVDet series [13, 14] uses Lift-splat-shot (LSS) [38] to generate the BEV feature and designs a BEV encoder with Feature Pyramid Network (FPN) to make more robust BEV features. SOLO-Fusion [35] further exploits long-term temporal modeling, achieving significant improvements.

Sparse query-based methods avoid the process of constructing dense BEV features. DETR3D [49] initializes a sparse query set and progressively refines object bounding box predictions through 3D-to-2D projection. PETR series [27, 28] introduces 3D positional encoding, enabling the model to encode multi-view 2D features into 3D features without the need of projecting. However, the global attention in PETR is dense and computational heavy. To address

<sup>1</sup>FPS is measured on a V100 GPU with the PyTorch backend.

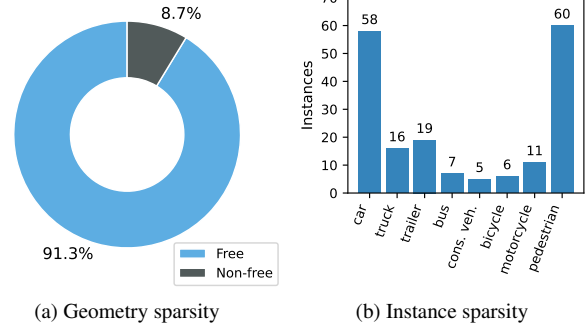


Figure 2. Two kinds of sparsity in 3D occupancy for autonomous driving. (a) We select a scene with the fewest empty voxels, but found that they still accounted for over 90% of the total. (b) We calculate the maximum number of instances contained in a single scene, with each category counted separately, and find that a small number of queries is enough to predict all objects.

this issue, SparseBEV [26] exploits a fully sparse architecture, achieving better performance than dense BEV-based methods while maintaining fast inference speed.

**Camera-based 3D Occupancy Prediction.** Occupancy Networks were originally proposed by Mescheder *et al.* [31, 37], focusing on continuously representing objects in 3D space. Recent variations in occupancy networks [1, 4, 41, 45, 47, 48] have shifted their focus to reconstructing 3D space and predicting voxel-level semantic information from image inputs. MonoScene [4] completes scene occupancy through a 2D and 3D UNet [39] connected by a sight projection module. OccNet [41] exploits applying universal occupancy features to various downstream tasks and introduces the OpenOcc benchmark. SurroundOcc [50] proposes a coarse-to-fine architecture for occupancy prediction. However, the large number of voxel queries is computational heavy. TPVFormer [15] proposes using tri-perspective view representations to supplement vertical structural information, but this inevitably leads to information loss. VoxFormer [21] initializes sparse queries based on monocular depth prediction. However, VoxFormer is not fully sparse as it still requires a sparse-to-dense MAE [11] module to complete the scene. There are also some methods emerged in the CVPR 2023 occupancy challenge [9, 23, 34], but none of them exploits a fully sparse design.

**End-to-end 3D Reconstruction from Posed Images.** 3D reconstruction aims to recover the 3D geometry of objects or scenes based on one or multiple posed images. Recently, some researchers have shifted their focus towards more compact and efficient end-to-end 3D reconstruction methods [2, 10, 33, 42, 43]. Atlas [33] extracts features from multi-view input images and maps them to 3D space to con-

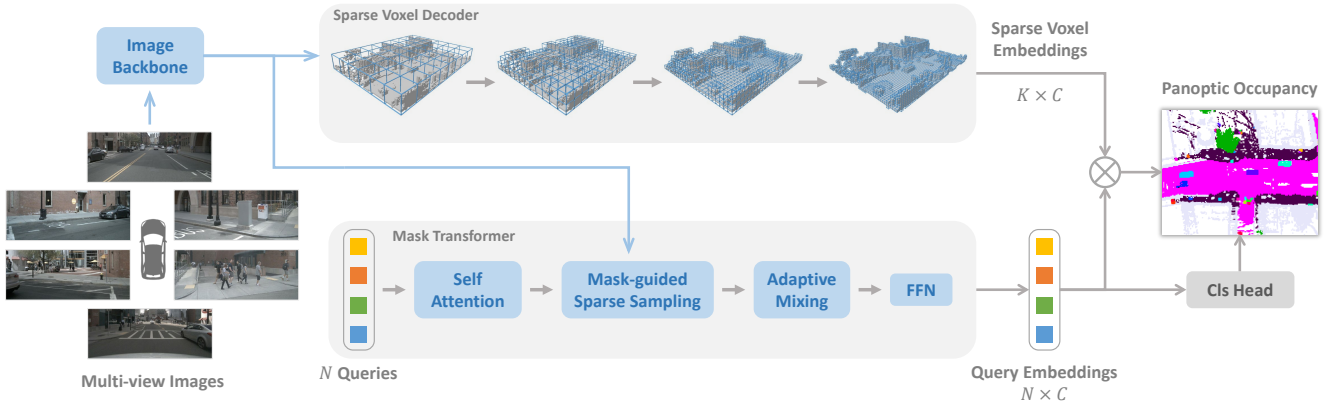


Figure 3. SparseOcc is a fully sparse architecture since it neither relies on dense 3D feature, nor has sparse-to-dense and global attention operations. The sparse voxel decoder reconstructs the sparse geometry of the scene, consisting of  $K$  voxels ( $K \ll W \times H \times D$ ). The mask transformer then uses  $N$  sparse instance queries to predict the mask and label of each object.

struct voxel features. The features are then regressed into a truncated signed distance function (TSDF) [7] for representing the reconstructed 3D space. NeuralRecon [43] directly reconstructs local surfaces represented as sparse TSDF volumes and uses a GRU-based TSDF fusion module to fuse features from previous fragments. To further address occlusion issues in multiple-view images, VoRTX [42] utilizes transformers to model interdependencies among multi-view images and aggregates their features. CVRecon [10] takes a different approach by avoiding occlusion-sensitive perspective mappings of 2D to 3D and directly uses cost volumes to establish 3D features from 2D image features.

**Mask Transformer.** In recent years, researchers have attempted to employ a unified segmentation model to handle both semantic and instance segmentation concurrently. Cheng *et al.* proposes a mask classification model named MaskFormer [6] to unify semantic and instance segmentation in terms of model architecture, loss functions, and training strategies. Building upon this, Mask2Former [5] further introduces masked attention, restricting the receptive field of attention based on instance masks, leading to improved performance. Inspired by the success of MaskFormer series, Mask3D [40] introduces mask transformer into point cloud instance segmentation achieves state-of-the-art performance without the need for intricate manual design. Furthermore, OpenMask3D [44] defines the open-vocabulary 3D instance segmentation task and proposes a model for zero-shot 3D segmentation.

### 3. SparseOcc

SparseOcc is a vision-centric occupancy model that only requires camera input. As shown in Fig. 3, SparseOcc has three modules: an image encoder consisting of an im-

age backbone and FPN [24], which extract 2D features from multi-view images; a sparse voxel decoder (Sec. 3.1), which predicts a sparse class-agnostic 3D occupancy and the embedding of each voxel from the image features; a mask transformer decoder (Sec 3.2), which further distinguishes semantics and instances in the predicted sparse 3D space.

#### 3.1. Sparse Voxel Decoder

Since the ground truth of 3D occupancy is a dense 3D volume of shape  $W \times H \times D$  (e.g.  $200 \times 200 \times 16$ ), previous methods typically build a dense 3D feature of shape  $W \times H \times D \times C$ , which is not computationally friendly. However, in our statistics, we found that over 90% of the voxels in the scene are free. This motivates us to generate a sparse 3D representation that only models the non-free areas of the scene, thereby saving computational resources.

**Overall architecture.** Our designed sparse voxel decoder is shown in Fig. 4. In general, it follows a coarse-to-fine structure but takes a sparse set of voxel tokens as input. At the end of each layer, we estimate an occupancy score for each voxel and sparsify based on the predicted score. Here we have two ways of sparsification, one is based on a threshold (e.g., only keeps score  $> 0.5$ ), and the other is based on top- $k$ . In this work we choose top- $k$ , because thresholding would cause samples with unequal length, affecting training efficiency.  $k$  is a dataset-related parameter, obtained by counting the maximum number of non-free voxels in each sample at different resolutions. The voxel tokens after sparsification will serve as the input for the next layer.

**Detailed design.** Within each layer, we use a transformer-like architecture to handle voxel-level queries, because the

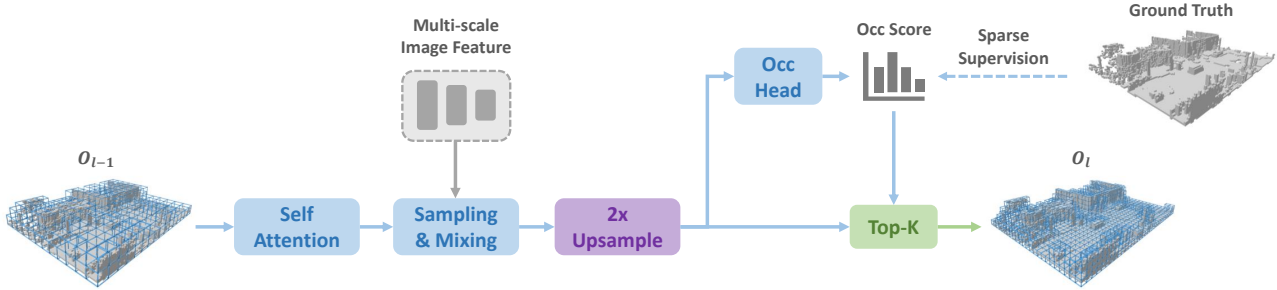


Figure 4. The detailed architecture of sparse voxel decoder, which follows a coarse-to-fine pipeline with three layers. Within each layer, we use a transformer-like architecture for 3D-2D interaction. At the end of each layer, it upsamples each voxels by  $2\times$  and estimates the probability of being occupied for each voxel.

transformer can handle unordered sets and is GPU-friendly. The concrete architecture is inspired by SparseBEV [26], which is an object detection method using a sparse scheme. The input to layer  $l$  consists of  $K_{l-1}$  voxel queries, each of them consists of the 3D location of the voxel and a  $C$ -dim content vector. These voxel queries are first processed by self attention to aggregate local and global features. Then, we use a linear layer to generate a set of 3D sampling offsets  $\{(\Delta x_i, \Delta y_i, \Delta z_i)\}$  from the content vector. These sampling offsets are transformed to sampling points in global coordinates according to the location and size of the voxel. Finally, we project these sampling points to each view using the provided camera intrinsics and extrinsics. Multi-scale features are sampled by bilinear interpolation in the image plane and further enhanced by adaptive mixing [16, 46].

**Temporal modeling.** Previous dense occupancy methods [14, 22, 41] typically warp the history BEV/3D feature to the current timestamp, and use deformable attention [55] or 3D convolutions to fuse temporal information. However, this approach is not applicable in our case, since our 3D feature is sparse. To handle this, we leverage the flexibility of sampling points by warping them to previous timestamps to sample the image feature. The sampled features from multiple timestamps are stacked and aggregated by adaptive mixing.

**Supervision.** We give supervision to each layer. Since we are reconstructing a class-agnostic occupancy in this step, we use binary cross entropy (BCE) loss to supervise the occupancy head. We only supervise a sparse set of locations from the predicted occupancy, which means the regions discarded in early stages will not be supervised.

Moreover, due to the severe class imbalance, the model can be easily dominated by categories with a large proportion, such as the ground, thereby ignoring other important elements in the scene, such as cars, people, etc. Therefore, voxels belonging to different classes are assigned with dif-

ferent loss weights. For example, voxels belonging to class  $c$  are assigned with a loss weight of:

$$w_c = \frac{\sum_{i=1}^C M_i}{M_c}, \quad (1)$$

where  $M_i$  is the number of voxels belonging to the  $i$ -th class in ground truth.

### 3.2. Mask Transformer

Our mask transformer is inspired by Mask2Former [5], which uses  $N$  sparse instance queries decoupled by binary mask query  $\mathbf{Q}_m \in [0, 1]^{N \times K}$  and content vector  $\mathbf{Q}_c \in \mathbb{R}^{N \times C}$ . The mask transformer consists of three steps: multi-head self attention (MHSA), mask-guided sparse sampling, and adaptive mixing. MHSA is used for the interaction between different queries as the common practice. Mask-guided sparse sampling and adaptive mixing are responsible for the interaction between queries and 2D image features.

**Mask-guided sparse sampling.** A simple baseline of mask transformer is to use the masked cross attention module in Mask2Former. However, it attends to all positions of the key, which can be very computation heavy. Here, we designed a simple alternative. Given the mask prediction of the previous  $(l - 1)$ -th Transformer decoder layer, we generate a set of 3D sampling points by randomly choosing the voxels inside the mask. These sampling points are projected to the image to sample image features. Besides, our sparse sampling mechanism makes the temporal modeling easier by simply warping the sampling points (as done in the sparse voxel decoder).

**Prediction.** For class prediction, we apply a linear classifier with a sigmoid activation based on the query embeddings  $\mathbf{Q}_c$ . For mask prediction, the query embeddings are converted to mask embeddings by a MLP. The mask embeddings  $\mathbf{M} \in \mathbb{R}^{Q \times C}$  have the same shape as query embed-

dings  $\mathbf{Q}_c$  and are dot-producted with the sparse voxel embeddings  $\mathbf{V} \in \mathbb{R}^{K \times C}$  to produce mask predictions. Thus, the prediction space of our mask transformer is constrained to the sparsified 3D space from the sparse voxel decoder, rather than the full 3D scene. The mask predictions will serve as the mask query  $\mathbf{Q}_m$  for the next layer.

**Supervision.** The reconstruction result from the sparse voxel decoder may not be reliable, as it may overlook or inaccurately detect certain elements. Thus, supervising the mask transformer presents certain challenges since its predictions are confined within this unreliable space. In cases of missed detection, where some ground truth instances are absent in the predicted sparse occupancy, we opt to discard these instances to prevent confusion. As for inaccurately detected elements, we simply categorize them as an additional “no object” category.

**Loss Functions.** Follow MaskFormer [6], we match the ground truth with the predictions using Hungarian matching. Focal loss  $L_{focal}$  is used for classification, while a combination of DICE loss [32]  $L_{dice}$  and BCE mask loss  $L_{mask}$  is used for mask prediction. Thus, the total loss of SparseOcc is composed of:

$$L = L_{focal} + L_{mask} + L_{dice} + L_{occ}, \quad (2)$$

where  $L_{occ}$  is the loss of sparse voxel decoder.

#### 4. Panoptic Occupancy Benchmark

To evaluate our method, we utilize the object bounding boxes from the 3D detection task to generate the panoptic occupancy ground truth. First, we define eight instance categories (including `car`, `truck`, `construction_vehicle`, `bus`, `trailer`, `motorcycle`, `bicycle`, `pedestrian`) and ten semantic categories (including `terrain`, `manmade`, `vegetation`, etc). Next, we identify each instance segment by grouping the voxels inside the box based on an existing semantic occupancy benchmark.

However, we observe that using the original size of the box for grouping may cause some boundary voxels being missed due to the compactness of the box. Enlarging the box (such as 1.2x) leads to excessive overlap between boxes. To address these issues, we designed a two-stage grouping scheme. In the first stage, we use the original size of the box for grouping. Then, for voxels that have not been assigned to a specific instance, we select the closest box and assign it. This scheme effectively resolves the problems of boundary omission and box overlap.

For evaluation metrics, we adopt the well-known panoptic quality (PQ) [17] metric, which is defined as the multiplication of *segmentation quality* (SQ) and *recognition quality* (RQ):

$$PQ = \underbrace{\frac{\sum_{(p,g) \in TP} \text{IoU}(p,g)}{|TP|}}_{\text{segmentation quality (SQ)}} \times \underbrace{\frac{|TP|}{|TP| + \frac{1}{2}|FP| + \frac{1}{2}|FN|}}_{\text{recognition quality (RQ)}}, \quad (3)$$

where the threshold of IoU between prediction  $p$  and ground-truth  $g$  is set to 0.5.

## 5. Experiments

We evaluate our model on the Occ3D-nus [45] dataset. Occ3D-nus is based on the nuScenes [3] dataset, which consists of large-scale multimodal data collected from 6 surround-view cameras, 1 lidar and 5 radars. The dataset has 1000 videos and is split into 700/150/150 videos for training/validation/testing. Each video has roughly 20s duration and the key samples are annotated every 0.5s.

For 3D occupancy prediction, the official evaluation metric is mean Intersection over Union (mIoU) to evaluate the semantic segmentation performance. We also add the metric of panoptic quality (PQ) to evaluation.

### 5.1. Implementation Details

We implement our model using PyTorch [36]. Following previous methods, we adopt ResNet-50 [12] as the image backbone. The mask transformer consists of 3 layers and weights are shared across different layers. By default, we use  $T = 8$  frames in total and the interval between adjacent frames is about 0.5s.

During training, we use the AdamW [29] optimizer with a global batch size of 8. The initial learning rate is set to  $2 \times 10^{-4}$  and is decayed with cosine annealing policy. For all experiments, we train our models for 24 epochs. FPS is measured on a Tesla V100 GPU with the PyTorch backend (single batch size).

### 5.2. Main Results

In Tab. 1, we compare SparseOcc with previous state-of-the-art methods on the validation split of Occ3D-nus. Our SparseOcc outperforms all previous methods by a large margin without using the visibility mask during training. Moreover, previous methods typically adopt ResNet101-DCN [8, 12] as the backbone, and the input size is set to  $1600 \times 900$ . We instead use a much smaller backbone of ResNet50 and a resolution of  $704 \times 256$ . SparseOcc can achieve the same or even higher performance than previous methods under a weaker setting, which clearly demonstrates the superiority of our solution.

Next, we construct a lite version of SparseOcc for faster speed. The channel dimension is reduced from 256 to 128, and the adaptive mixing is replaced with deformable attention. As shown in Tab. 2, SparseOcc can achieve  $2 \times$  FPS (up to 25.4 FPS on V100) at the expense of only 1.0 mIoU.

Method	Backbone	Input Size	mIoU																	
				others	barrier	bicycle	bus	car	cons. veh.	motor.	pedes.	ttc. cone	trailer	truck	drv. surf.	other flat	sidewalk	terrain	manmade	vegetation
MonoScene [4]	R101	1600×900	6.1	1.8	7.2	4.3	4.9	9.4	5.7	4.0	3.0	5.9	4.5	7.2	14.9	6.3	7.9	7.4	1.0	7.7
OccFormer [54]	R101	1600×900	21.9	5.9	30.3	12.3	34.4	39.2	14.4	16.5	17.2	9.3	13.9	26.4	51.0	31.0	34.7	22.7	6.8	7.0
BEVFormer [22]	R101	1600×900	26.9	5.9	37.8	17.9	40.4	42.4	7.4	23.9	21.8	21.0	22.4	30.7	55.4	28.4	36.0	28.1	20.0	17.7
CTF-Occ [45]	R101	1600×900	28.5	8.1	39.3	20.6	38.3	42.2	16.9	24.5	22.7	21.1	23.0	31.1	53.3	33.8	38.0	33.2	20.8	18.0
TPVFormer [15]	R101	1600×900	27.8	7.2	38.9	13.7	40.8	45.9	17.2	20.0	18.9	14.3	26.7	34.2	55.7	35.5	37.6	30.7	19.4	16.8
SparseOcc (1f)	R50	704×256	27.0	8.8	33.2	17.1	34.4	41.0	16.1	19.2	20.8	21.0	18.4	27.9	62.4	31.0	39.2	35.1	17.5	16.8
SparseOcc (8f)	R50	704×256	<b>30.9</b>	10.6	39.2	20.2	32.9	43.3	19.4	23.8	23.4	29.3	21.4	29.3	67.7	36.3	44.6	40.9	22.0	21.9

Table 1. 3D occupancy prediction performance on the Occ3D-nuScenes [45] dataset. “8f” means fusing temporal information from 7+1 frames. Our method achieves the same or even higher performance than previous methods under a weaker setting.

Voxel Decoder	IoU	mIoU	FPS
SparseOcc (1f)	<b>42.9</b>	<b>27.0</b>	12.7
SparseOcc-lite (1f)	41.1	26.0	<b>25.4</b>

Table 2. Optimized model for faster inference speed. SparseOcc can achieve 2× FPS without sacrificing too much accuracy.

Voxel Decoder	IoU	mIoU	FPS
Dense coarse-to-fine	38.8	<b>27.7</b>	3.3
Dense patch-based	37.1	25.1	4.1
Sparse coarse-to-fine	<b>42.9</b>	27.0	<b>12.7</b>

Table 3. Sparse voxel decoder vs. dense voxel decoder. Our sparse voxel decoder achieves nearly 4× faster inference speed than the dense counterparts.

We further provide qualitative results in Fig. 5. Despite discarding over 90% of the voxels, SparseOcc is still able to effectively model the geometric structure of the scene and capture fine-grained objects.

### 5.3. Ablations

In this section, we conduct ablations on the validation split of Occ3D-nus to confirm the effectiveness of each module. The default choice for our model is colored **gray**.

**Sparse voxel decoder vs. dense voxel decoder.** In Tab. 3, we compare our sparse voxel decoder to the dense counterparts. Here, we implement two baselines, and both of them output a dense  $200 \times 200 \times 16 \times C$  feature map. One is a coarse-to-fine architecture without dropping the empty voxels. We also replace self attention with 3D convolution and use 3D deconvolution to upsample the predictions following SurroundOcc [50]. The other is a patch-based architecture by dividing the 3D space into a small number

Cross Attention	IoU	mIoU	FPS
Dense cross attention	42.2	26.8	8.7
Sparse sampling	42.8	23.2	<b>12.7</b>
+ Mask-guided	<b>42.9</b>	<b>27.0</b>	<b>12.7</b>

Table 4. Ablation of the cross attention module in mask transformer. Mask-guided sparse sampling is stronger and faster than the dense cross attention.

of patches, similar to PETRv2 [28] for BEV segmentation. We use  $25 \times 25 \times 2 = 1250$  queries and each one of them corresponds to a specific patch of shape  $8 \times 8 \times 8$ . A stack of deconvolution layers then lift the coarse queries to a full-resolution 3D volume.

As we can see from the table, the dense coarse-to-fine baseline achieves good performance of 27.7 mIoU and 38.8 IoU but running slowly at 3.3 FPS. The patch-based one slightly improves the inference speed to 4.1 FPS but severely hurts the performance by 2.6 mIoU. Instead, our sparse voxel decoder produces sparse 3D features in the shape of  $K \times C$  (where  $K = 65536 \ll 200 \times 200 \times 16$ ), achieving an inference speed that is nearly 4× faster than the counterparts. Moreover, it has achieved the highest IoU of 42.9, and a comparable mIoU of 27.0. This demonstrates the necessity and effectiveness of our sparse design.

#### Mask-guided sparse sampling vs. dense cross attention.

In the mask transformer of SparseOcc, we propose mask-guided sparse sampling for 3D-2D interaction. Here, we compare our design with global cross attention as it is the common practice in MaskFormer and Mask3D. As shown in Tab. 4, our sparse sampling mechanism is 50% faster than dense cross attention. Furthermore, we find that constraining the sampling points to the foreground region of the predicted mask is crucial and leads to a +3.8 mIoU improvement over the baseline which generates sampling points uni-

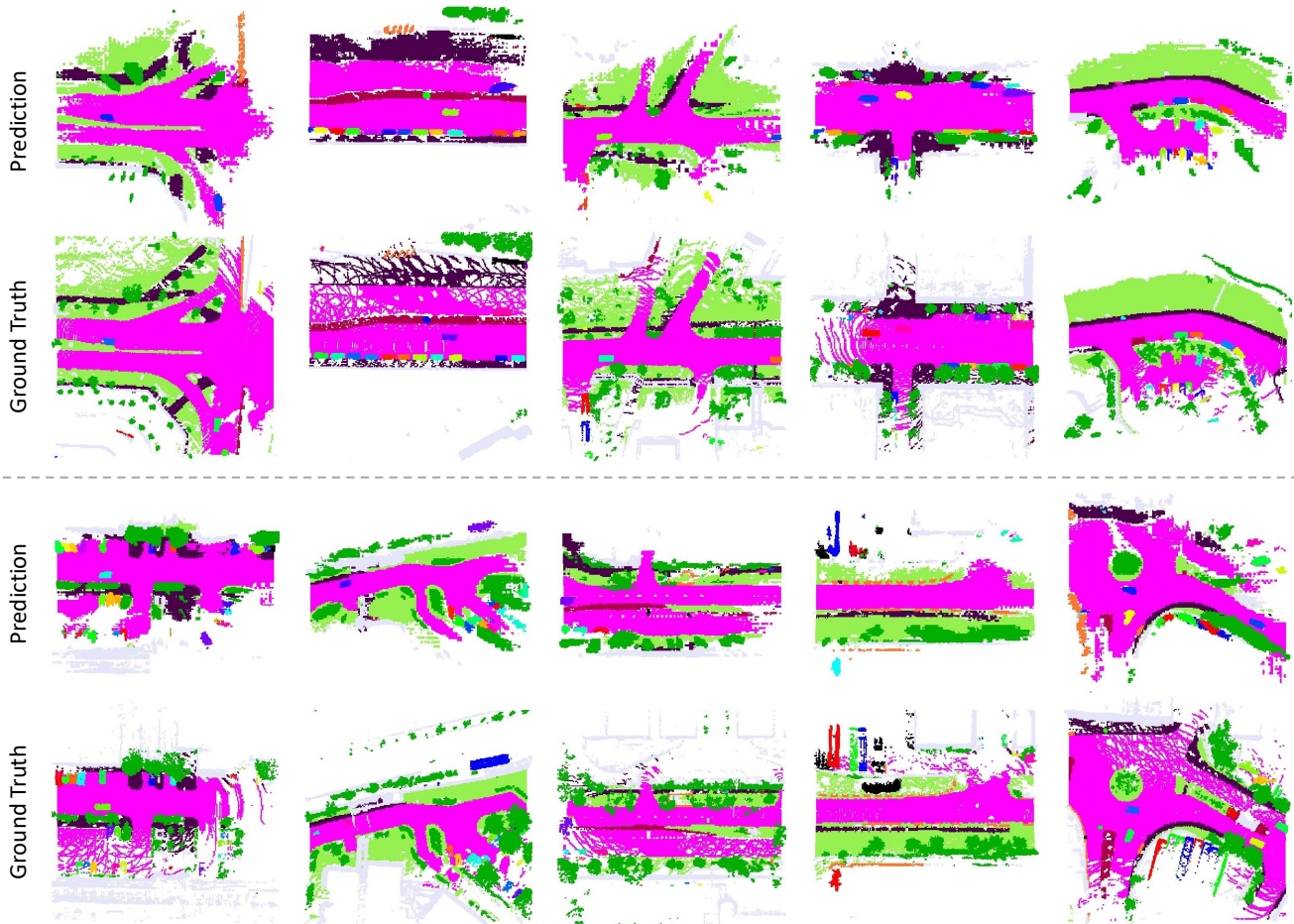


Figure 5. Visualization of panoptic occupancy prediction. Different instances are distinguished by colors. Our model can capture fine-grained objects and road structure in the scene.

Supervision	IoU	mRecall
Binary cross entropy	28.5	24.2
+ 2-class balanced (free/non-free)	36.4	35.4
+ 18-class balanced	<b>42.3</b>	<b>74.9</b>

Table 5. Ablation of the supervision of sparse voxel decoder. Class balance is crucial even for class-agnostic reconstruction tasks.

formly in the entire 3D space.

**Is a limited set of voxels predicted by the sparse voxel decoder sufficient to cover the scene?** Here, we further study the reconstruction performance of the sparse voxel decoder. Since it yields class-agnostic predictions, we cannot use the mIoU metric to measure its performance, and can only use the IoU metric. However, since the GT contains annotations of 18 classes, we also use the mRecall metric, which averages the recall rate among all classes.

As shown in Tab. 5, using vanilla binary cross entropy loss to supervise the sparse voxel decoder can only achieve a performance of 28.5 IoU and 24.2 mRecall. Next, we balance the weight of positive and negative voxels accordingly and achieve an improved performance of 36.4 IoU and 35.4 mRecall. By further balancing the weight of all 18 classes, the mRecall is doubled to 74.9, demonstrating that a limited number of voxel tokens is sufficient to cover the scene.

**Temporal modeling.** In Tab. 6, we validate the effectiveness of temporal fusion. From rows 1-4 of the table, we can see that the temporal modeling of SparseOcc is very effective, with performance steadily increasing as the number of frames increases. Since we fuse temporal information in both the sparse voxel decoder (SVD) and the mask transformer (MT), we further conduct ablations in rows 5-6 of the table. The experiments prove that the temporal fusion in both places contributes to the final performance. The temporal fusion at the sparse voxel decoder will significantly

Temporal Fusion		Frames	IoU	mIoU	PQ
SVD	MT				
-	-	1	42.9	27.0	8.9
✓	✓	2	44.1	28.4	9.6
✓	✓	4	46.0	29.6	10.7
✓	✓	8	<b>48.6</b>	<b>31.4</b>	<b>12.4</b>
-	✓	8	43.1	27.9	9.7
✓	-	8	48.4	31.1	11.8

Table 6. Ablation of temporal modeling. The first two columns indicate whether we fuse temporal information in sparse voxel decoder (SVD) or mask transformer (MT).

Number of Queries	IoU	mIoU	PQ
50	-	-	-
100	<b>42.9</b>	<b>27.0</b>	8.9
300	42.7	27.0	8.5
500	42.6	26.9	8.2

Table 7. Number of queries in mask transformer. Increasing the number of queries brings no improvement to the final performance.

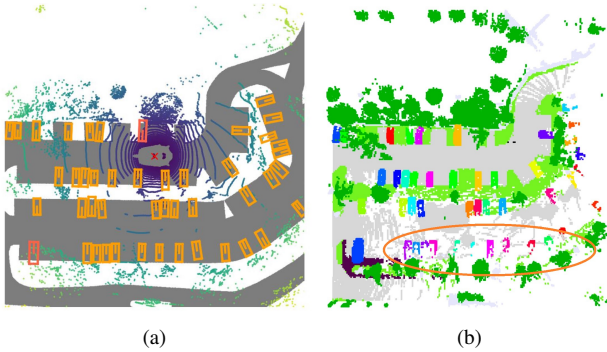


Figure 6. Ground truth comparison between 3D detection (a) and 3D panoptic occupancy (b). The occupancy ground truth acquired by accumulated point cloud is not reliable and contains lots of broken objects (see the orange marker).

impair the performance by 3.5 mIoU and 2.7 PQ; while the temporal fusion at the mask transformer has a relatively minor impact on performance (0.3 mIoU and 0.6 PQ).

**Number of queries in mask transformer.** We also ablate the number of queries in Tab. 7. The training crashes when we use 50 queries since the number of ground-truth instances exceeds 50 in some scenes. We find that 100 queries are enough in our case, as further increasing the number of queries brings no improvement.

## 6. Limitations

**Ground truth is unreliable.** Current occupancy datasets on the market are all implemented based on accumulated LiDAR point clouds. This approach can lead to areas not scanned by LiDAR being mistakenly considered free, as shown in Fig. 6. Although Occ3D-nus uses a visibility mask to evaluate only the visible parts, it overlooks the model’s ability of **scene completion**, thereby degrading the occupancy task into a depth estimation task. This is why the leaderboard of Occ3D-nus is dominated by depth-based methods. We would like to kindly point out that it may misguide the occupancy community.

**Accumulative errors.** In order to implement a fully sparse architecture, we discard a large number of empty voxels in the early stages. However, empty voxels that are mistakenly discarded cannot be recovered in subsequent stages. Moreover, the prediction of the mask transformer is constrained within a space predicted by the sparse voxel decoder. Some ground-truth instances do not appear in this unreliable space, leading to inadequate training of the mask transformer.

## 7. Conclusion

In this paper, we have proposed a fully sparse panoptic occupancy network, named SparseOcc, which neither relies on dense 3D feature, nor has sparse-to-dense and global attention operations. SparseOcc exploits geometric and instance sparsity via sparse voxel decoder and mask transformer respectively. We also created the first vision-centric panoptic occupancy benchmark. Experiments show that SparseOcc achieves the state-of-the-art performance on Occ3D-nus for both speed and accuracy. We hope this exciting result will attract more attention to the fully sparse 3D occupancy paradigm.

**Acknowledgements.** This work is supported by National Key R&D Program of China (No. 2022ZD0160900), National Natural Science Foundation of China (No. 62076119, No. 61921006), Fundamental Research Funds for the Central Universities (No. 020214380091, No. 020214380099), and Collaborative Innovation Center of Novel Software Technology and Industrialization. Besides, we would like to thank Hongyang Li and Tianyu Li for their profound discussions.

## References

- [1] Tesla AI Day. <https://www.youtube.com/watch?v=j0z4FweCy4M>, 2021. 1, 2
- [2] Aljaz Bozic, Pablo Palafox, Justus Thies, Angela Dai, and Matthias Nießner. Transformerfusion: Monocular rgb scene

- reconstruction using transformers. *Advances in Neural Information Processing Systems*, 34:1403–1414, 2021. 2
- [3] Holger Caesar, Varun Bankiti, Alex H Lang, Sourabh Vora, Venice Erin Liong, Qiang Xu, Anush Krishnan, Yu Pan, Giancarlo Baldan, and Oscar Beijbom. nuscenes: A multi-modal dataset for autonomous driving. In *Proceedings of the IEEE/CVF conference on computer vision and pattern recognition*, pages 11621–11631, 2020. 5
- [4] Anh-Quan Cao and Raoul de Charette. Monoscene: Monocular 3d semantic scene completion. In *Proceedings of the IEEE/CVF Conference on Computer Vision and Pattern Recognition*, pages 3991–4001, 2022. 2, 6
- [5] Bowen Cheng, Ishan Misra, Alexander G Schwing, Alexander Kirillov, and Rohit Girdhar. Masked-attention mask transformer for universal image segmentation. In *Proceedings of the IEEE/CVF Conference on Computer Vision and Pattern Recognition*, pages 1290–1299, 2022. 3, 4
- [6] Bowen Cheng, Alex Schwing, and Alexander Kirillov. Pixel classification is not all you need for semantic segmentation. *Advances in Neural Information Processing Systems*, 34:17864–17875, 2021. 3, 5
- [7] Brian Curless and Marc Levoy. A volumetric method for building complex models from range images. In *Proceedings of the 23rd annual conference on Computer graphics and interactive techniques*, pages 303–312, 1996. 3
- [8] Jifeng Dai, Haozhi Qi, Yuwen Xiong, Yi Li, Guodong Zhang, Han Hu, and Yichen Wei. Deformable convolutional networks. In *Proceedings of the IEEE international conference on computer vision*, pages 764–773, 2017. 5
- [9] Yangyang Ding, Luying Huang, and Jiachen Zhong. Multi-scale occ: 4th place solution for Proceedings of the IEEE/CVF Conference on Computer Vision and Pattern Recognition 2023 3d occupancy prediction challenge. *arXiv preprint arXiv:2306.11414*, 2023. 2
- [10] Ziyue Feng, Liang Yang, Pengsheng Guo, and Bing Li. Cvrecon: Rethinking 3d geometric feature learning for neural reconstruction. In *Proceedings of the IEEE/CVF International Conference on Computer Vision*, pages 17750–17760, 2023. 2, 3
- [11] Kaiming He, Xinlei Chen, Saining Xie, Yanghao Li, Piotr Dollár, and Ross Girshick. Masked autoencoders are scalable vision learners. In *Proceedings of the IEEE/CVF conference on computer vision and pattern recognition*, pages 16000–16009, 2022. 2
- [12] Kaiming He, Xiangyu Zhang, Shaoqing Ren, and Jian Sun. Deep residual learning for image recognition. In *Proceedings of the IEEE conference on computer vision and pattern recognition*, pages 770–778, 2016. 5
- [13] Junjie Huang and Guan Huang. Bevdet4d: Exploit temporal cues in multi-camera 3d object detection. *arXiv preprint arXiv:2203.17054*, 2022. 2
- [14] Junjie Huang, Guan Huang, Zheng Zhu, and Dalong Du. Bevdet: High-performance multi-camera 3d object detection in bird-eye-view. *arXiv preprint arXiv:2112.11790*, 2021. 1, 2, 4
- [15] Yuanhui Huang, Wenzhao Zheng, Yunpeng Zhang, Jie Zhou, and Jiwen Lu. Tri-perspective view for vision-based 3d semantic occupancy prediction. In *Proceedings of the IEEE/CVF Conference on Computer Vision and Pattern Recognition*, pages 9223–9232, 2023. 2, 6
- [16] Xu Jia, Bert De Brabandere, Tinne Tuytelaars, and Luc V Gool. Dynamic filter networks. *Advances in neural information processing systems*, 29, 2016. 4
- [17] Alexander Kirillov, Kaiming He, Ross Girshick, Carsten Rother, and Piotr Dollár. Panoptic segmentation. In *Proceedings of the IEEE/CVF conference on computer vision and pattern recognition*, pages 9404–9413, 2019. 2, 5
- [18] Alex H Lang, Sourabh Vora, Holger Caesar, Lubing Zhou, Jiong Yang, and Oscar Beijbom. Pointpillars: Fast encoders for object detection from point clouds. In *Proceedings of the IEEE/CVF conference on computer vision and pattern recognition*, pages 12697–12705, 2019. 1
- [19] Hongyang Li, Yang Li, Huijie Wang, Jia Zeng, Pinlong Cai, Huilin Xu, Dahua Lin, Junchi Yan, Feng Xu, Lu Xiong, Jingdong Wang, Futang Zhu, Kai Yan, Chunjing Xu, Tiancai Wang, Beipeng Mu, Shaoqing Ren, Zhihui Peng, and Yu Qiao. Open-sourced data ecosystem in autonomous driving: the present and future. *arXiv preprint arXiv:2312.03408*, 2023. 2
- [20] Hongyang Li, Chonghao Sima, Jifeng Dai, Wenhai Wang, Lewei Lu, Huijie Wang, Jia Zeng, Zhiqi Li, Jiazhi Yang, Hanming Deng, et al. Delving into the devils of bird’s-eye-view perception: A review, evaluation and recipe. *IEEE Transactions on Pattern Analysis and Machine Intelligence*, 2023. 2
- [21] Yiming Li, Zhiding Yu, Christopher Choy, Chaowei Xiao, Jose M Alvarez, Sanja Fidler, Chen Feng, and Anima Anandkumar. Voxformer: Sparse voxel transformer for camera-based 3d semantic scene completion. In *Proceedings of the IEEE/CVF Conference on Computer Vision and Pattern Recognition*, pages 9087–9098, 2023. 1, 2
- [22] Zhiqi Li, Wenhai Wang, Hongyang Li, Enze Xie, Chonghao Sima, Tong Lu, Yu Qiao, and Jifeng Dai. Bevformer: Learning bird’s-eye-view representation from multi-camera images via spatiotemporal transformers. In *European Conference on Computer Vision (ECCV)*, pages 1–18. Springer, 2022. 1, 2, 4, 6
- [23] Zhiqi Li, Zhiding Yu, David Austin, Mingsheng Fang, Shiyi Lan, Jan Kautz, and Jose M Alvarez. Fb-occ: 3d occupancy prediction based on forward-backward view transformation. *arXiv preprint arXiv:2307.01492*, 2023. 1, 2
- [24] Tsung-Yi Lin, Piotr Dollár, Ross Girshick, Kaiming He, Bharath Hariharan, and Serge Belongie. Feature pyramid networks for object detection. In *Proceedings of the IEEE conference on computer vision and pattern recognition*, pages 2117–2125, 2017. 3
- [25] Haisong Liu, Tao Lu, Yihui Xu, Jia Liu, and Limin Wang. Learning optical flow and scene flow with bidirectional camera-lidar fusion. *arXiv preprint arXiv:2303.12017*, 2023. 1
- [26] Haisong Liu, Yao Teng, Tao Lu, Haiguang Wang, and Limin Wang. Sparsebev: High-performance sparse 3d object detection from multi-camera videos. In *Proceedings of the IEEE/CVF International Conference on Computer Vision*, pages 18580–18590, 2023. 2, 4

- [27] Yingfei Liu, Tiancai Wang, Xiangyu Zhang, and Jian Sun. PETR: position embedding transformation for multi-view 3d object detection. In *European Conference on Computer Vision (ECCV)*, pages 531–548. Springer, 2022. 2
- [28] Yingfei Liu, Junjie Yan, Fan Jia, Shuailin Li, Qi Gao, Tiancai Wang, Xiangyu Zhang, and Jian Sun. Petrv2: A unified framework for 3d perception from multi-camera images. *arXiv preprint arXiv:2206.01256*, 2022. 2, 6
- [29] Ilya Loshchilov and Frank Hutter. Decoupled weight decay regularization. In *International Conference on Learning Representations (ICLR)*, 2019. 5
- [30] Tao Lu, Xiang Ding, Haisong Liu, Gangshan Wu, and Limin Wang. Link: Linear kernel for lidar-based 3d perception. In *Proceedings of the IEEE/CVF Conference on Computer Vision and Pattern Recognition*, pages 1105–1115, 2023. 1
- [31] Lars Mescheder, Michael Oechsle, Michael Niemeyer, Sebastian Nowozin, and Andreas Geiger. Occupancy networks: Learning 3d reconstruction in function space. In *Proceedings of the IEEE/CVF conference on computer vision and pattern recognition*, pages 4460–4470, 2019. 2
- [32] Fausto Milletari, Nassir Navab, and Seyed-Ahmad Ahmadi. V-net: Fully convolutional neural networks for volumetric medical image segmentation. In *2016 fourth international conference on 3D vision (3DV)*, pages 565–571. Ieee, 2016. 5
- [33] Zak Murez, Tarrence Van As, James Bartolozzi, Ayan Sinha, Vijay Badrinarayanan, and Andrew Rabinovich. Atlas: End-to-end 3d scene reconstruction from posed images. In *Computer Vision–ECCV 2020: 16th European Conference, Glasgow, UK, August 23–28, 2020, Proceedings, Part VII 16*, pages 414–431. Springer, 2020. 2
- [34] Mingjie Pan, Jiaming Liu, Renrui Zhang, Peixiang Huang, Xiaoqi Li, Li Liu, and Shanghang Zhang. Renderocc: Vision-centric 3d occupancy prediction with 2d rendering supervision. *arXiv preprint arXiv:2309.09502*, 2023. 2
- [35] Jinhyung Park, Chenfeng Xu, Shijia Yang, Kurt Keutzer, Kris Kitani, Masayoshi Tomizuka, and Wei Zhan. Time will tell: New outlooks and a baseline for temporal multi-view 3d object detection. *arXiv preprint arXiv:2210.02443*, 2022. 2
- [36] Adam Paszke, Sam Gross, Francisco Massa, Adam Lerer, James Bradbury, Gregory Chanan, Trevor Killeen, Zeming Lin, Natalia Gimelshein, Luca Antiga, et al. Pytorch: An imperative style, high-performance deep learning library. *Advances in neural information processing systems*, 32:8026–8037, 2019. 5
- [37] Songyou Peng, Michael Niemeyer, Lars Mescheder, Marc Pollefeys, and Andreas Geiger. Convolutional occupancy networks. In *Computer Vision–ECCV 2020: 16th European Conference, Glasgow, UK, August 23–28, 2020, Proceedings, Part III 16*, pages 523–540. Springer, 2020. 2
- [38] Jonah Philion and Sanja Fidler. Lift, splat, shoot: Encoding images from arbitrary camera rigs by implicitly unprojecting to 3d. In *Computer Vision–ECCV 2020: 16th European Conference, Glasgow, UK, August 23–28, 2020, Proceedings, Part XIV 16*, pages 194–210. Springer, 2020. 2
- [39] Olaf Ronneberger, Philipp Fischer, and Thomas Brox. U-net: Convolutional networks for biomedical image segmentation. In *Medical Image Computing and Computer-Assisted Intervention–MICCAI 2015: 18th International Conference, Munich, Germany, October 5-9, 2015, Proceedings, Part III 18*, pages 234–241. Springer, 2015. 2
- [40] Jonas Schult, Francis Engelmann, Alexander Hermans, Or Litany, Siyu Tang, and Bastian Leibe. Mask3d: Mask transformer for 3d semantic instance segmentation. In *2023 IEEE International Conference on Robotics and Automation (ICRA)*, pages 8216–8223. IEEE, 2023. 3
- [41] Chonghao Sima, Wenwen Tong, Tai Wang, Li Chen, Silei Wu, Hanming Deng, Yi Gu, Lewei Lu, Ping Luo, Dahua Lin, and Hongyang Li. Scene as occupancy. 2023. 1, 2, 4
- [42] Noah Stier, Alexander Rich, Pradeep Sen, and Tobias Höllerer. Vortx: Volumetric 3d reconstruction with transformers for voxelwise view selection and fusion. In *2021 International Conference on 3D Vision (3DV)*, pages 320–330. IEEE, 2021. 2, 3
- [43] Jiaming Sun, Yiming Xie, Linghao Chen, Xiaowei Zhou, and Hujun Bao. Neuralrecon: Real-time coherent 3d reconstruction from monocular video. In *Proceedings of the IEEE/CVF Conference on Computer Vision and Pattern Recognition*, pages 15598–15607, 2021. 2, 3
- [44] Ayça Takmaz, Elisabetta Fedele, Robert W Sumner, Marc Pollefeys, Federico Tombari, and Francis Engelmann. Openmask3d: Open-vocabulary 3d instance segmentation. *arXiv preprint arXiv:2306.13631*, 2023. 3
- [45] Xiaoyu Tian, Tao Jiang, Longfei Yun, Yue Wang, Yilun Wang, and Hang Zhao. Occ3d: A large-scale 3d occupancy prediction benchmark for autonomous driving. *arXiv preprint arXiv:2304.14365*, 2023. 2, 5, 6
- [46] Ilya O Tolstikhin, Neil Houlsby, Alexander Kolesnikov, Lucas Beyer, Xiaohua Zhai, Thomas Unterthiner, Jessica Yung, Andreas Steiner, Daniel Keysers, Jakob Uszkoreit, et al. Mlp-mixer: An all-mlp architecture for vision. *Advances in Neural Information Processing Systems*, 34:24261–24272, 2021. 4
- [47] Xiaofeng Wang, Zheng Zhu, Wenbo Xu, Yunpeng Zhang, Yi Wei, Xu Chi, Yun Ye, Dalong Du, Jiwen Lu, and Xingang Wang. Openoccupancy: A large scale benchmark for surrounding semantic occupancy perception. *arXiv preprint arXiv:2303.03991*, 2023. 2
- [48] Yuqi Wang, Yuntao Chen, Xingyu Liao, Lue Fan, and Zhaoxiang Zhang. Panoocc: Unified occupancy representation for camera-based 3d panoptic segmentation. *arXiv preprint arXiv:2306.10013*, 2023. 2
- [49] Yue Wang, Vitor Campagnolo Guizilini, Tianyuan Zhang, Yilun Wang, Hang Zhao, and Justin Solomon. Detr3d: 3d object detection from multi-view images via 3d-to-2d queries. In *Conference on Robot Learning*, pages 180–191. PMLR, 2022. 2
- [50] Yi Wei, Linqing Zhao, Wenzhao Zheng, Zheng Zhu, Jie Zhou, and Jiwen Lu. Surroundocc: Multi-camera 3d occupancy prediction for autonomous driving. In *Proceedings of the IEEE/CVF International Conference on Computer Vision*, pages 21729–21740, 2023. 1, 2, 6
- [51] Zetong Yang, Yanan Sun, Shu Liu, and Jiaya Jia. 3dssd: Point-based 3d single stage object detector. In *Proceedings of the IEEE/CVF conference on computer vision and pattern recognition*, pages 11040–11048, 2020. 1

- [52] Zetong Yang, Yanan Sun, Shu Liu, Xiaoyong Shen, and Jiaya Jia. Std: Sparse-to-dense 3d object detector for point cloud. In *Proceedings of the IEEE/CVF international conference on computer vision*, pages 1951–1960, 2019. 1
- [53] Tianwei Yin, Xingyi Zhou, and Philipp Krahenbuhl. Center-based 3d object detection and tracking. In *Proceedings of the IEEE/CVF conference on computer vision and pattern recognition*, pages 11784–11793, 2021. 1
- [54] Yunpeng Zhang, Zheng Zhu, and Dalong Du. Occformer: Dual-path transformer for vision-based 3d semantic occupancy prediction. *arXiv preprint arXiv:2304.05316*, 2023. 6
- [55] Xizhou Zhu, Weijie Su, Lewei Lu, Bin Li, Xiaogang Wang, and Jifeng Dai. Deformable detr: Deformable transformers for end-to-end object detection. *arXiv preprint arXiv:2010.04159*, 2020. 4